Thickness dependence of dynamic magnetic properties of soft (FeCo)-Si alloy thin films

Shuang Wu,[1,2] Kyotaro Abe,[1,3] Takuma Nakano,[3] Tim Mewes,[1,2] Claudia Mewes,[1,2] G. J. Mankey,[1,2] and Takao Suzuki[1,4,5]
[1]*Center for Materials for Information Technology, The University of Alabama, Tuscaloosa, Alabama 35487, USA*
[2]*Department of Physics and Astronomy, The University of Alabama, Tuscaloosa, Alabama 35487, USA*
[3]*Materials Development Center, TDK Corporation, Narita 286-0805, Japan*
[4]*Department of Metallurgical and Materials Engineering, The University of Alabama, Tuscaloosa, Alabama 35487, USA*
[5]*Department of Electrical and Computer Engineering, The University of Alabama, Tuscaloosa, Alabama 35487, USA*

(Received 3 December 2018; revised manuscript received 2 April 2019; published 19 April 2019)

$Fe_{69}Co_{26}Si_5$ alloy thin films of various thicknesses were deposited on MgO(100) single crystal substrates by magnetron sputtering at 230 °C substrate temperature. The thickness dependence of the dynamic magnetic properties was investigated using broadband ferromagnetic resonance (FMR). The x-ray diffraction results indicate that all films are of the bcc structure with an in-plane epitaxial alignment of $[100]_{FeCoSi} /\!/ [110]_{MgO}$. The exchange constant was determined from the field shift between the uniform precession FMR mode and the first order perpendicular standing spin wave resonance mode in the FMR spectra. The effective damping parameter decreases dramatically with increasing film thickness up to 16 nm due to the decrease of the spin pumping contribution and then remains relatively constant as the film thickness increases. In-plane angle dependent FMR measurements reveal that the in-plane anisotropy of these films is dominated by a fourfold magnetic anisotropy, which increases sharply with increasing film thickness up to 16 nm and then shows a slightly decreasing trend as the film thickness increases. In-plane angular dependence of the FMR linewidth shows a strong two-magnon scattering contribution.

DOI: 10.1103/PhysRevB.99.144416

I. INTRODUCTION

High frequency applications such as magnetic recording head and antenna require soft magnetic materials with high saturation magnetization, high permeability, low coercivity, and low damping parameter. Fe-Co based alloys such as Fe-Co-Al, Fe-Co-Si, and Fe-Co-Si-Al were investigated by several groups both in bulk and thin films because of their high saturation magnetization and low coercivity [1–5]. So far, very few studies on the magnetization dynamics of these materials can be found in the literature. However, understanding of the magnetization dynamics of soft magnetic thin film is essential for improving their high frequency performance. Both quasistatic and dynamic magnetic properties of (FeCo)-Al alloy thin films as functions of Al content, film thickness, and growth temperature have been studied [6–8]. An effective damping parameter as low as 0.0004 was found for an 83 nm thick $Fe_{73}Co_{25}Al_2$ thin film, which is in good agreement with the value reported by Schoen *et al.* [9] for $Fe_{75}Co_{25}$ alloy thin film. In this paper, a systematic study on the thickness dependence of the dynamic magnetic properties of $Fe_{69}Co_{26}Si_5$ alloy thin films is presented; additional information about the quasistatic properties of these films can be found in Ref. [10].

II. EXPERIMENTAL METHOD

Multilayers of $[Fe(0.3\ nm)/Fe_{66}Co_{34}(1.0\ nm)/Si(0.1\ nm)] \times N$ were deposited on MgO(100) single crystal substrates using a dc magnetron sputtering system. The chamber was pumped down to a base pressure lower than 2×10^{-7} Torr and the films were sputtered using 4 mTorr of Ar pressure. The deposition rates for Fe, $Fe_{66}Co_{34}$, and Si were 0.12, 0.15, and 0.026 nm/s, respectively. The substrate temperature during the deposition was 230 °C. A 5 nm thick Ru capping layer was deposited for protection purposes. A small in-plane magnetic field of 50 Oe was applied during the deposition along the ⟨110⟩ direction of $Fe_{69}Co_{26}Si_5$.

The film thicknesses t were determined by x-ray reflectivity. The structural properties were characterized by x-ray diffraction (XRD) with Cu K_α radiation. The morphology of the films including the alloying of the stack was studied using cross-sectional TEM/EDX of the films [10]. The quasistatic magnetic properties were measured using a vibrating sample magnetometer (VSM) and a magneto-optical Kerr effect (MOKE) system and have been reported in Ref. [10]. The dynamic properties were determined using broadband ferromagnetic resonance (FMR) covering a frequency range from 12 to 66 GHz. In-plane angle dependent FMR measurements were carried out at 30 GHz to determine the in-plane anisotropy of the samples.

III. RESULTS AND DISCUSSION

A. Structural and quasistatic magnetic properties

Figure 1 shows the XRD patterns for $Fe_{69}Co_{26}Si_5$ thin films with various thicknesses. The films show a broad (200) bcc peak around $2\theta = 65°$; the corresponding (110) bcc peak of the $Fe_{69}Co_{26}Si_5$ film and the (200) peak of the MgO substrate are so close that only one peak can be observed around $2\theta = 43°$. The low angle in-plane XRD pattern of the 60 nm thick sample shows four (200) bcc peaks separated by 90°. The (200) peaks of MgO substrate are shifted by 45° with

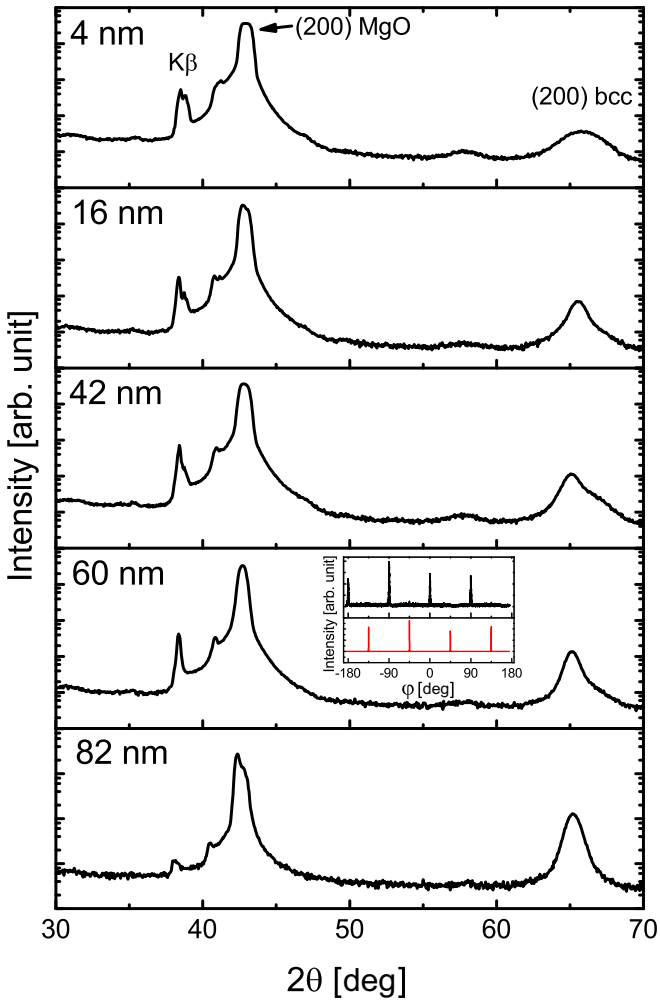

FIG. 1. XRD patterns for $Fe_{69}Co_{26}Si_5$ thin films with various thicknesses. Inset: low angle in-plane XRD patterns for the 60 nm thick film (black line in the top part) and MgO substrate (red line in the bottom part).

respect to the (200) peaks of the sample film, which indicates that $[110]_{FeCoSi} /\!/ [100]_{MgO}$.

The hysteresis loops measured along $[1\bar{1}0]$, [100], or [110] directions are shown in Fig. 2(a). The observed hysteresis curves are consistent with a fourfold in-plane anisotropy with easy axes along the ⟨100⟩ directions. The thickness dependence of coercivity H_c, saturation magnetization M_s, and the remanence to saturation magnetization ratio M_r/M_s are shown in Fig. 2(b). H_c significantly increases from 4 to 16 nm and decreases with further increasing thickness. M_s, on the other hand, slightly increases from 4 to 16 nm and only slightly decreases with further increasing thickness. M_r/M_s shows a slight decrease with increasing thickness across the whole thickness range. The details of the quasistatic magnetic properties are discussed elsewhere [10].

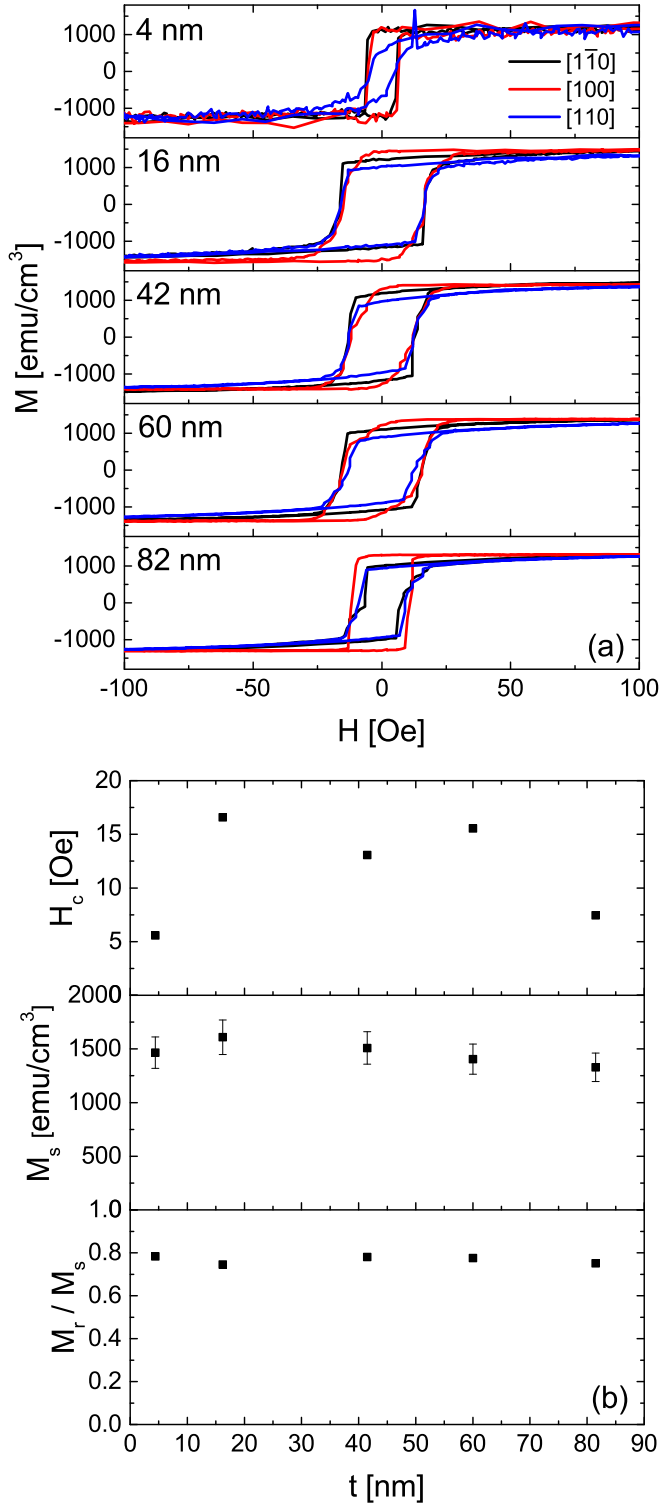

FIG. 2. (a) Hysteresis loops for $Fe_{69}Co_{26}Si_5$ thin films with various thicknesses measured by VSM. The magnetic field is applied in the $[1\bar{1}0]$, [100], or [110] direction. (b) Thickness dependence of coercivity H_c, saturation magnetization M_s, and the remanence to saturation magnetization ratio M_r/M_s for $Fe_{69}Co_{26}Si_5$ thin films. All the values are measured along $[1\bar{1}0]$.

B. Dynamic magnetic properties

1. FMR theoretical model

The coordinates we use in this paper are shown in Fig. 3. When the external magnetic field is applied along an arbitrary in-plane angle ϕ_H, the equilibrium in-plane angle of the magnetization is denoted as ϕ_M. In our model we include a uniaxial anisotropy field $H_u = \frac{2K_u}{M_s}$ and a fourfold anisotropy

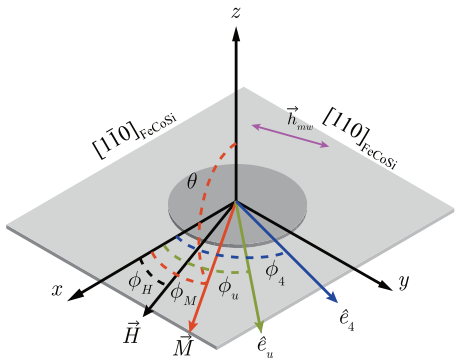

FIG. 3. Sketch of the in-plane angle dependent FMR measurements geometry. All magnetic fields and the magnetization $\vec{M}$ are in the film plane. The external field $\vec{H}$ is applied along the direction of angle ϕ_H. The microwave field $\vec{h}_{mw}$ is perpendicular to the external field. $\hat{e}_u$ and $\hat{e}_4$ represent the directions of the easy axes of the uniaxial and fourfold anisotropy field, respectively. ϕ_u and ϕ_4 stand for the in-plane angles of the easy axis of the uniaxial and fourfold anisotropy with the x axis, respectively. The equilibrium in-plane angle of the magnetization is ϕ_M.

field $H_4 = \frac{4K_4}{M_s}$ with easy axes along in-plane angles ϕ_u and ϕ_4, respectively. K_u and K_4 stand for the uniaxial and fourfold anisotropy constants, respectively. The dispersion relation for the uniform precession FMR mode in such a system is given by [11]

$$\left(\frac{f}{\gamma'}\right)^2 = H_a \cdot H_b,$$

with

$$\begin{aligned} H_a &= H_{\text{res}}\cos(\phi_M-\phi_H) + \frac{H_4}{2}\cos 4(\phi_M-\phi_4) \\ &\quad + H_u\cos 2(\phi_M-\phi_u), \\ H_b &= H_{\text{res}}\cos(\phi_M-\phi_H) + \frac{H_4}{8}[3+\cos 4(\phi_M-\phi_4)] \\ &\quad + \frac{H_u}{2}[1+\cos 2(\phi_M-\phi_u)] + 4\pi M_{\text{eff}}, \end{aligned} \tag{1}$$

where f is the frequency of the microwave field, $\gamma' = \frac{g\mu_B}{h}$ is the gyromagnetic ratio, H_{res} is the resonance field, $4\pi M_{\text{eff}} = 4\pi M_s - 2\frac{K_\perp}{M_s}$ is the effective magnetization, and $K_\perp$ accounts for any perpendicular anisotropy present in the films. We did our broadband FMR measurements along the $[1\bar{1}0]$ direction, which is the in-plane hard axis. To obtain a simpler equation for the analysis of the broadband FMR measurements, the uniaxial anisotropy is ignored ($H_u = 0$) since it is much weaker compared to the fourfold anisotropy. Because the external field $\vec{H}$ is applied along the hard axis and exceeds the saturation field in the broadband FMR measurements, we have $\phi_M - \phi_H = 0$; thus $\cos 4(\phi_M - \phi_4) = -1$. Substituting the above conditions into Eq. (1), we arrive at a simplified equation for broadband FMR measurements along the hard axis as follows:

$$\left(\frac{f}{\gamma'}\right)^2 = \left(H_{\text{res}} - \frac{H_4}{2}\right)\left(H_{\text{res}} + \frac{H_4}{4} + 4\pi M_{\text{eff}}\right). \tag{2}$$

Perpendicular standing spin waves (PSSW) are commonly observed in FMR experiments. The dispersion relation for spin waves can be written in a similar form as Eq. (1) [12–14]:

$$\left(\frac{f}{\gamma'}\right)^2 = (H_a + H_{\text{ex}})(H_b + H_{\text{ex}}), \tag{3}$$

with the exchange field $H_{\text{ex}} = \frac{2A}{M_s}(\frac{n\pi}{t})^2$, where A is the exchange constant, n is the spin wave mode number, and t is the film thickness. Similarly, Eq. (3) can be simplified to

$$\left(\frac{f}{\gamma'}\right)^2 = \left(H_{\text{res}} - \frac{H_4}{2} + H_{\text{ex}}\right)\left(H_{\text{res}} + \frac{H_4}{4} + 4\pi M_{\text{eff}} + H_{\text{ex}}\right) \tag{4}$$

when the external field is along an in-plane hard axis.

2. *FMR measurement results*

A representative FMR spectrum of the 82 nm thick film measured at 40 GHz along the $[1\bar{1}0]$ direction is shown in Fig. 4(a). Two resonances are visible in this spectrum. The stronger one at 7.1 kOe is the FMR mode and the weaker one at 6.6 kOe is the first order PSSW mode. This PSSW mode can be observed for all samples except the thinnest one, where the expected large field separation and small signal strength of the PSSW mode prevented its detection. The field dependence of the resonance frequency for the 82 nm thick film is shown in Fig. 4(b). By fitting the two modes simultaneously using Eq. (4), we can obtain the exchange constant A. The extracted exchange constants range from 15 to 25 pJ/m [see Fig. 4(c)], which is comparable with the reported values of $Fe_{65}Co_{35}$ (17 pJ/m) [15] and Co_2FeSi (31.5 pJ/m) [16]. The variations in A are probably due to the finite spin pinning at the surface caused by an additional surface anisotropy and magnetization inhomogeneity close to the interfaces of the film [17,18].

Figure 5(a) shows the linewidth as a function of microwave frequency, which for all samples shows a linear relationship. The linewidth of the thinnest sample is significantly larger than for the other four samples. The frequency dependencies of the linewidth in the figure are fitted using the following equation [19–22]:

$$\Delta H = \Delta H_0 + \frac{2}{\sqrt{3}}\frac{\alpha_{\text{eff}}}{\gamma'}f, \tag{5}$$

where ΔH_0 is the inhomogeneous broadening and α_{eff} is the effective damping parameter. The extracted α_{eff} are shown in Fig. 5(b). The upper limit of the effective damping parameter, as indicated by the asymmetric error bars, can be determined by assuming that the linewidth at the highest frequency is caused solely by a Gilbert-like linewidth contribution. This approach provides a conservative estimate for the upper limit of the error margins of the effective damping parameter even for cases where two-magnon scattering or inhomogeneous broadening contribute significantly to the linewidth. The effective damping parameter decreases drastically from the 4 nm to the 16 nm thick film. Then it stays in the range between 0.002 and 0.003. The effective damping parameter we extracted here contains both intrinsic and extrinsic contributions such as two-magnon scattering [23,24], eddy-current damping [25,26], and radiative damping [26,27]. The intrinsic damping will be lower than the effective damping, especially those of

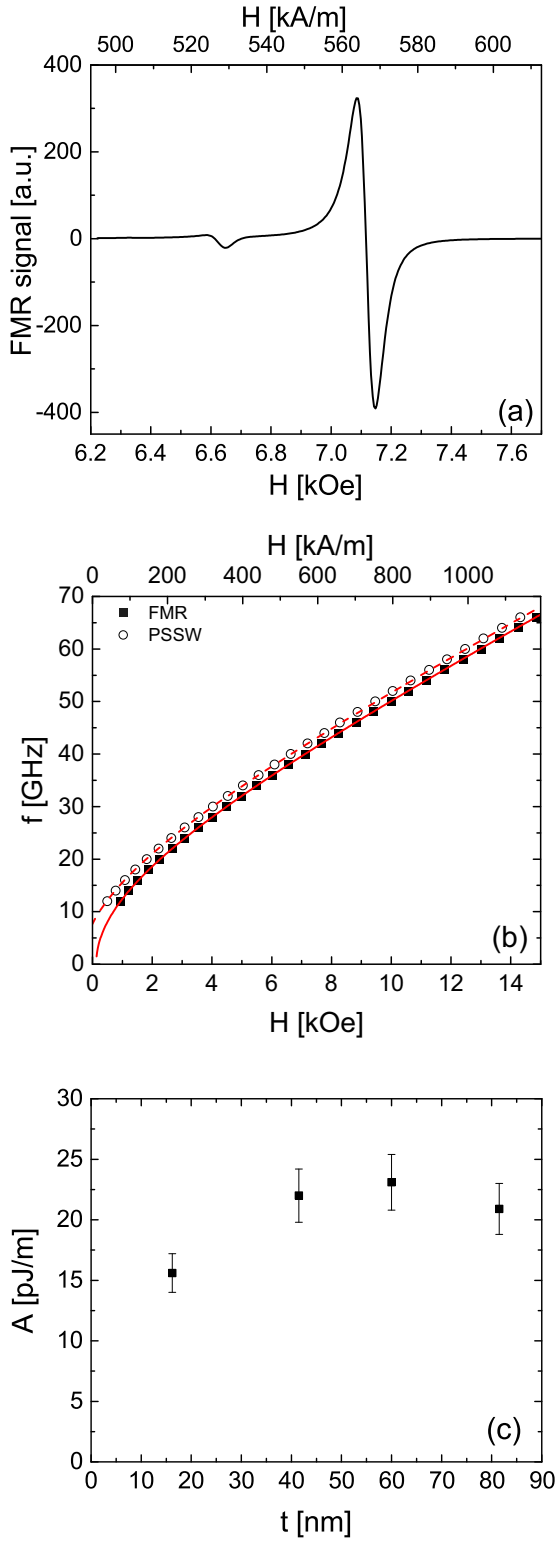

FIG. 4. (a) FMR spectrum at 40 GHz and (b) Kittel plot for the 82 nm thick $Fe_{69}Co_{26}Si_5$ thin film measured along $[1\bar{1}0]$. Red lines correspond to fits to the data using Eq. (4) with $n = 0$ and $n = 1$. (c) Estimation of exchange constant A for $Fe_{69}Co_{26}Si_5$ thin films except the thinnest one.

the thicker samples, which suffer from a larger eddy-current damping.

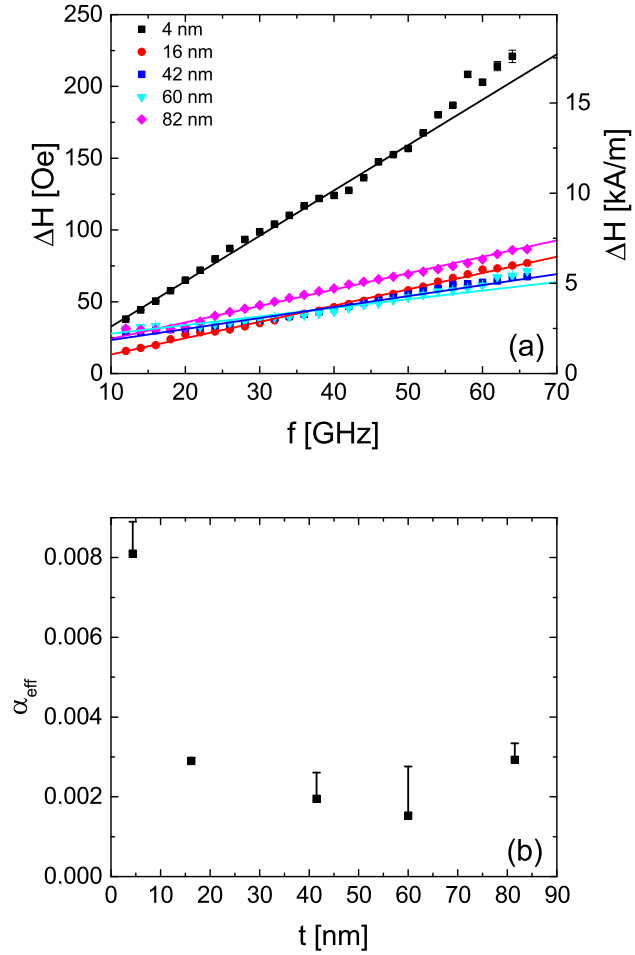

FIG. 5. (a) FMR linewidth as a function of resonance frequency f for $Fe_{69}Co_{26}Si_5$ thin films with various thicknesses. Lines correspond to fits to the data. (b) Thickness dependence of effective damping parameter. The upper limits are determined from the highest frequency data points and the origin.

The significant increase of the effective damping parameter increase for the 4 nm thick film has two potential origins: two-magnon scattering and spin pumping. A rough estimation of the spin pumping contribution to the effective parameter for the 4 nm thick film using [28] $\alpha_{sp} = \frac{\gamma'}{4\pi M_s}\frac{h}{t}g^{\uparrow\downarrow}$ gives a value of $\alpha_{sp} \approx 0.01$. Here h is the Planck constant and $g^{\uparrow\downarrow}$ is the spin mixing conductance. In this estimate we have assumed that the 5 nm Ru cap layer is a perfect spin sink, which based on reported spin diffusion lengths [29] appears to be a reasonable assumption. So far no spin mixing conductance values have been reported for FeCoSi/Ru bilayer systems in the literature. However, the reported $g^{\uparrow\downarrow}$ values for similar ferromagnet/nonmagnetic metal bilayer systems such as CoFeB/Pt (4×10^{15} cm^{-2}) [30], NiFe/Ru (3.8×10^{15} cm^{-2}) [28], and CoFe/Pt (4.0×10^{15} cm^{-2}) [31] are very close despite the material differences in each system. Thus we expect the spin mixing conductance of our system to be of the same order and used $g^{\uparrow\downarrow} \approx 4.0 \times 10^{15}$ cm^{-2} in our estimate. Since the estimated spin pumping contribution of the 4 nm thick film is of the same order as the measured effective damping parameter, the two-magnon scattering is unlikely to be responsible for the huge increase of the effective damping

parameter of the 4 nm thick film. As will be shown in the following paragraphs, this interpretation is consistent with our results from in-plane angle dependent FMR measurements. In fact, the measurement direction for the broadband FMR investigations was chosen to minimize the two-magnon scattering contribution.

The result of the quasistatic magnetization reversal and broadband FMR measurements suggests the presence of an in-plane anisotropy. In order to get a better understanding of the anisotropy in these films, in-plane angle dependent FMR measurements were carried out. Figure 6(a) exemplarily shows the in-plane angular dependence of the resonance field and linewidth for the 82 nm thick film. The resonance field and the linewidth show a clear fourfold symmetry, which is consistent with the crystal symmetry of $Fe_{69}Co_{26}Si_5$ and its epitaxial growth on MgO. In angular dependent FMR measurements, minima of the resonance field indicate an easy axis, whereas maxima correspond to hard axes. Therefore, the easy axes of the fourfold anisotropy are along the ⟨100⟩ directions of $Fe_{69}Co_{26}Si_5$, consistent with the quasistatic magnetic properties; see Fig. 2 and Ref. [10]. Close inspection of the difference of the residual using a purely fourfold fit, i.e., the angular dependence of the measured resonance field and a fit using only a fourfold anisotropy term in Eq. (1), reveals the presence of a very small uniaxial anisotropy in the films. The easy axis of the small uniaxial anisotropy is not aligned with the easy axis of the fourfold anisotropy; furthermore, the easy axis varies from sample to sample. Such a small uniaxial anisotropy can for example be caused by the presence of a slight inclination during deposition [32].

Angles where the resonance field has maxima are minima for the linewidth and vice versa. To quantitatively analyze the anisotropies, we fit the resonance fields of the FMR and PSSW modes using Eq. (3) with $n = 0$ and $n = 1$, respectively. The extracted values of H_u and H_4 as a function of the film thickness are shown in Fig. 6(b). The uniaxial anisotropy fields are smaller than 25 Oe for all samples and do not show a systematic thickness dependence. The dominating fourfold anisotropy increases sharply from 4 nm to 16 nm, then shows a decreasing trend as the film thickness increases. This kind of fourfold anisotropy thickness dependency was also observed in epitaxial Fe(001) thin films and can be explained using Néel's pair model [33]. In this model the nonmonotonous thickness dependence of the fourfold anisotropy is caused by an interfacial contribution due to the broken symmetry and lattice misfit strain that influences the anisotropy through magnetoelastic coupling [33,34]. The differences between the anisotropy fields determined form the FMR mode and those determined from the PSSW mode can be attributed to an inhomogeneous fourfold anisotropy across the film thickness. Due to the different mode profiles for the FMR and PSSW modes the two modes weigh the anisotropy distribution across the film thickness differently, leading to the observed differences in the measured anisotropy fields. It is worth pointing out that inhomogeneities of the crystalline anisotropy can also be a source of two-magnon scattering that is not interfacial in nature; see, for example, Refs. [20,35]. A broad distribution of magnetic inhomogeneities, as indicated by the differences between FMR and PSSW modes, in turn will lead to a broad frequency range over which the two-magnon contribution

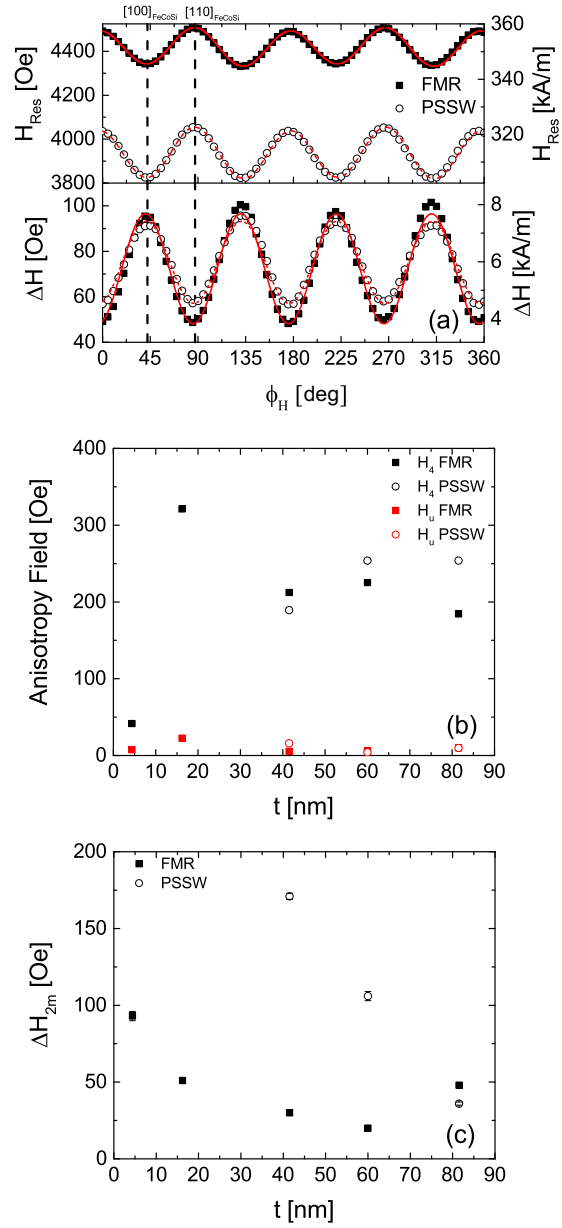

FIG. 6. (a) In-plane angular dependence of the resonance field and linewidth for the 82 nm thick $Fe_{69}Co_{26}Si_5$ film at 30 GHz. The solid squares and open circles represent the FMR mode and PSSW mode, respectively. Red lines in the upper plot correspond to fits to the data using Eq. (3) with $n = 0$ and $n = 1$; red lines in the bottom plot correspond to fits to the data using Eq. (6). (b) Thickness dependence of the uniaxial anisotropy and fourfold anisotropy. (c) Thickness dependence of the anisotropic linewidth contribution from two-magnon scattering.

to the linewidth is approximately linear with frequency; cf. Fig. 5.

The in-plane angular dependence of the FMR linewidth can be analyzed by considering the different contributions [36–39]: Gilbert damping, two-magnon scattering, linewidth broadening due to mosaicity, and inhomogeneous linewidth broadening. The inhomogeneous linewidth broadening caused by the fluctuation of the strength of the anisotropy fields is angle independent [37,40]. The in-plane angular dependence

of the linewidth contributions from the field drag effect and the linewidth broadening due to mosaicity for a fourfold anisotropy have an eightfold symmetry [36]. This leaves two-magnon scattering as the source of the observed fourfold in-plane angular dependence of the linewidth. For two-magnon scattering, misfit dislocations [41] in the crystalline structures, inhomogeneities of the crystalline anisotropy [20,35], and interfacial contributions due to roughness are all expected to reflect the crystal symmetry and hence show a fourfold in-plane angular dependence. Therefore, the in-plane angular dependence of the linewidth is fitted with [39]

$$\Delta H = \Delta H_{\text{iso}} + \Delta H_{2m} \cos^2[2(\phi - \phi_{2m})], \tag{6}$$

where ΔH_{iso} represents all isotropic contributions including inhomogeneous broadening, spin pumping, and Gilbert damping; ΔH_{2m} represents the anisotropic contribution from two-magnon scattering; $\phi_{2m} = 45^\circ$ represents the in-plane angle where the strength of the two-magnon scattering is maximum. The extracted values of ΔH_{2m} are plotted in Fig. 6(c) as a function of the film thickness. From the figure, one can see that ΔH_{2m} generally decreases with increasing film thickness. For a two-magnon scattering contribution of strictly interfacial origin, one expects this linewidth contribution to scale like the square of the inverse film thickness [9,18,23,26,42]. However, for this sample series, such a dependence is not observed. In particular, the thickest film exhibits a significantly larger ΔH_{2m} than what one would expect based on the rest of the series. This suggests that, in addition to the interfacial two-magnon scattering contribution, another contribution dominates the linewidth at larger film thicknesses. Two-magnon scattering from misfit dislocations [41] and inhomogeneities of the crystalline anisotropy [20,35] are possible mechanisms that are not interfacial in origin and thus do not necessarily decrease with increasing film thickness. Both will have the same symmetry as the crystal lattice, consistent with the observed fourfold symmetry of the linewidth. In particular, one expects the density of misfit dislocations to increase with increasing film thickness above a critical film thickness t_c [43], consistent with our observation of a larger two-magnon contribution for the thickest film.

IV. SUMMARY

The quasistatic and dynamic magnetic properties of $Fe_{69}Co_{26}Si_5$ alloy thin films of various thicknesses were studied using VSM and broadband FMR. The quasistatic magnetic properties such as saturation magnetization, coercivity, and the remanence to saturation magnetization ratio all show only a weak thickness dependence; for more details, see Ref. [10]. The dynamic measurements using broadband FMR and in-plane angle dependent measurements unambiguously show that [100] and [110] are the easy and hard axes, respectively, of the dominant fourfold anisotropy. The FMR measurements further enabled us to quantify the strength of the fourfold anisotropy. We also observed a very small in-plane uniaxial anisotropy. Based on the field shift between the FMR and the PSSW modes, the exchange constant of these films is estimated to be 20 ± 5 pJ/m. A strong fourfold in-plane anisotropy and a weak uniaxial anisotropy are observed in in-plane rotation FMR measurements. Both the effective damping parameter and the fourfold anisotropy show strong thickness dependence when the film thickness is below 16 nm. Finally, a fourfold symmetry was also observed in the linewidth vs in-plane angle plot, which can be attributed to two-magnon scattering.

ACKNOWLEDGMENTS

The present work is partially supported by the MINT/UA-TDK collaboration program. C.M. would like to acknowledge support through NSF-CAREER Award No. 1452670.

[1] H. Fujimori, M. Kikuchi, O. Yoshihisa, and T. Masumoto, Sci. Rep. Res. Inst. Tohoku Univ. A **26**, 36 (1976).
[2] M. Hayakawa, K. Hayashi, W. Ishikawa, Y. Ochiai, H. Matsuda, Y. Iwasaki, and K. Aso, IEEE Trans. Magn. **23**, 3092 (1987).
[3] K. Hayashi, M. Hayakawa, W. Ishikawa, Y. Ochiai, H. Matsuda, Y. Iwasaki, and K. Aso, J. Appl. Phys. **61**, 3514 (1987).
[4] T. Bitoh, A. Makino, A. Inoue, and A. L. Greer, Appl. Phys. Lett. **88**, 182510 (2006).
[5] H. Zuo, S. Ge, Z. Wang, Y. Xiao, and D. Yao, Scr. Mater. **62**, 766 (2010).
[6] I. Kanada, A. Cruce, T. Mewes, S. Wu, C. Mewes, G. Mankey, and T. Suzuki, AIP Adv. **7**, 056105 (2017).
[7] Y. Ariake, I. Kanada, T. Mewes, G. Mankey, Y. Tanaka, S. Wu, C. Mewes, and T. Suzuki, IEEE Trans. Magn. **53**, 1 (2017).
[8] Y. Ariake, S. Wu, I. Kanada, T. Mewes, Y. Tanaka, G. Mankey, C. Mewes, and T. Suzuki, AIP Adv. **8**, 056119 (2018).
[9] M. A. W. Schoen, D. Thonig, M. L. Schneider, T. J. Silva, H. T. Nembach, O. Eriksson, O. Karis, and J. M. Shaw, Nat. Phys. **12**, 839 (2016).
[10] K. Abe, S. Wu, Y. Tanaka, Y. Ariake, I. Kanada, T. Mewes, G. Mankey, C. Mewes, and T. Suzuki, AIP Adv. **9**, 035139 (2019).
[11] M. Belmeguenai, F. Zighem, Y. Roussigné, S.-M. Chérif, P. Moch, K. Westerholt, G. Woltersdorf, and G. Bayreuther, Phys. Rev. B **79**, 024419 (2009).
[12] C. Kittel, Phys. Rev. **110**, 1295 (1958).
[13] A. Martins, S. C. Trippe, A. D. Santos, and F. Pelegrini, J. Magn. Magn. Mater. **308**, 120 (2007).
[14] S. Klingler, A. V. Chumak, T. Mewes, B. Khodadadi, C. Mewes, C. Dubs, O. Surzhenko, B. Hillebrands, and A. Conca, J. Phys. D: Appl. Phys. **48**, 015001 (2014).
[15] X. Liu and A. Morisako, J. Appl. Phys. **103**, 07E726 (2008).
[16] G. Oksana, H. Jaroslav, T. Simon, H. Burkard, S. Horst, and J. Gerhard, J. Phys. D: Appl. Phys. **42**, 232001 (2009).
[17] E. Burgos, E. Sallica Leva, J. Gómez, F. Martinez Tabares, M. Vásquez Mansilla, and A. Butera, Phys. Rev. B **83**, 174417 (2011).
[18] P. Talagala, P. S. Fodor, D. Haddad, R. Naik, L. E. Wenger, P. P. Vaishnava, and V. M. Naik, Phys. Rev. B **66**, 144426 (2002).
[19] T. D. Rossing, J. Appl. Phys. **34**, 995 (1963).
[20] B. Heinrich, J. F. Cochran, and R. Hasegawa, J. Appl. Phys. **57**, 3690 (1985).
[21] Z. Celinski and B. Heinrich, J. Appl. Phys. **70**, 5935 (1991).

[22] C. K. A. Mewes and T. Mewes, in *Handbook of Nanomagnetism: Applications and Tools*, edited by R. A. Lukaszew (Pan Stanford Publishing, Singapore, 2015), Chap. 4, pp. 71–96.
[23] R. Arias and D. L. Mills, Phys. Rev. B **60**, 7395 (1999).
[24] R. Arias and D. L. Mills, J. Appl. Phys. **87**, 5455 (2000).
[25] Y. Li and W. E. Bailey, Phys. Rev. Lett. **116**, 117602 (2016).
[26] A. Kumar, F. Pan, S. Husain, S. Akansel, R. Brucas, L. Bergqvist, S. Chaudhary, and P. Svedlindh, Phys. Rev. B **96**, 224425 (2017).
[27] M. A. W. Schoen, J. M. Shaw, H. T. Nembach, M. Weiler, and T. J. Silva, Phys. Rev. B **92**, 184417 (2015).
[28] J. E. Gómez, B. Zerai Tedlla, N. R. Álvarez, G. Alejandro, E. Goovaerts, and A. Butera, Phys. Rev. B **90**, 184401 (2014).
[29] S. Yakata, Y. Ando, T. Miyazaki, and S. Mizukami, Jpn. J. Appl. Phys. **45**, 3892 (2006).
[30] A. Ruiz-Calaforra, T. Brächer, V. Lauer, P. Pirro, B. Heinz, M. Geilen, A. V. Chumak, A. Conca, B. Leven, and B. Hillebrands, J. Appl. Phys. **117**, 163901 (2015).
[31] A. Ganguly, K. Kondou, H. Sukegawa, S. Mitani, S. Kasai, Y. Niimi, Y. Otani, and A. Barman, Appl. Phys. Lett. **104**, 072405 (2014).
[32] R. D. McMichael, C. G. Lee, J. E. Bonevich, P. J. Chen, W. Miller, and W. F. Egelhoff, J. Appl. Phys. **88**, 5296 (2000).
[33] N. Tournerie, P. Schieffer, B. Lépine, C. Lallaizon, P. Turban, and G. Jézéquel, Phys. Rev. B **78**, 134401 (2008).
[34] P. Bertoncini, P. Wetzel, D. Berling, A. Mehdaoui, B. Loegel, G. Gewinner, R. Poinsot, and V. Pierron-Bohnes, J. Magn. Magn. Mater. **237**, 191 (2001).
[35] E. Schlömann, J. Phys. Chem. Solids **6**, 257 (1958).
[36] K. Lenz, H. Wende, W. Kuch, K. Baberschke, K. Nagy, and A. Jánossy, Phys. Rev. B **73**, 144424 (2006).
[37] K. Zakeri, J. Lindner, I. Barsukov, R. Meckenstock, M. Farle, U. von Hörsten, H. Wende, W. Keune, J. Rocker, S. S. Kalarickal *et al.*, Phys. Rev. B **76**, 104416 (2007).
[38] H. Kurebayashi, T. Skinner, K. Khazen, K. Olejník, D. Fang, C. Ciccarelli, R. Campion, B. Gallagher, L. Fleet, A. Hirohata *et al.*, Appl. Phys. Lett. **102**, 062415 (2013).
[39] S. Emori, U. S. Alaan, M. T. Gray, V. Sluka, Y. Chen, A. D. Kent, and Y. Suzuki, Phys. Rev. B **94**, 224423 (2016).
[40] B. Heinrich, in *Ultrathin Magnetic Structures III: Fundamentals of Nanomagnetism*, edited by J. A. C. Bland and B. Heinrich (Springer, Berlin, 2005), Chap. 5, pp. 143–210.
[41] G. Woltersdorf and B. Heinrich, Phys. Rev. B **69**, 184417 (2004).
[42] J. Beik Mohammadi, J. M. Jones, S. Paul, B. Khodadadi, C. K. A. Mewes, T. Mewes, and C. Kaiser, Phys. Rev. B **95**, 064414 (2017).
[43] S. M. Hu, J. Appl. Phys. **69**, 7901 (1991).